Adolescence is associated with genomically patterned consolidation of the hubs of the human brain connectome

Kirstie J. Whitaker[a,1,2], Petra E. Vértes[a,2], Rafael Romero-Garcia[a], František Váša[a], Michael Moutoussis[b], Gita Prabhu[b], Nikolaus Weiskopf[b,c], Martina F. Callaghan[b], Konrad Wagstyl[a], Timothy Rittman[d], Roger Tait[a], Cinly Ooi[a], John Suckling[a,e,f], Becky Inkster[a], Peter Fonagy[g], Raymond J. Dolan[b,h], Peter B. Jones[a,e], Ian M. Goodyer[a,e], the NSPN Consortium[3], and Edward T. Bullmore[a,e,f,i]

[a]Department of Psychiatry, University of Cambridge, Cambridge CB2 0SZ, United Kingdom; [b]Wellcome Trust Centre for Neuroimaging, University College London, London WC1N 3BG, United Kingdom; [c]Department of Neurophysics, Max Planck Institute for Human Cognitive and Brain Sciences, 04103 Leipzig, Germany; [d]Department of Clinical Neurosciences, University of Cambridge, Cambridge CB2 3EB, United Kingdom; [e]Cambridgeshire and Peterborough National Health Service Foundation Trust, Cambridge, CB21 5EF, United Kingdom; [f]Medical Research Council/Wellcome Trust Behavioural and Clinical Neuroscience Institute, University of Cambridge, Cambridge CB2 3EB, United Kingdom; [g]Research Department of Clinical, Educational and Health Psychology, University College London, London WC1E 6BT, United Kingdom; [h]Max Planck University College London Centre for Computational Psychiatry and Ageing Research, University College London, London WC1B 5EH, United Kingdom; and [i]ImmunoPsychiatry, GlaxoSmithKline Research and Development, Stevenage SG1 2NY, United Kingdom

How does human brain structure mature during adolescence? We used MRI to measure cortical thickness and intracortical myelination in 297 population volunteers aged 14–24 y old. We found and replicated that association cortical areas were thicker and less myelinated than primary cortical areas at 14 y. However, association cortex had faster rates of shrinkage and myelination over the course of adolescence. Age-related increases in cortical myelination were maximized approximately at the internal layer of projection neurons. Adolescent cortical myelination and shrinkage were coupled and specifically associated with a dorsoventrally patterned gene expression profile enriched for synaptic, oligodendroglial- and schizophrenia-related genes. Topologically efficient and biologically expensive hubs of the brain anatomical network had greater rates of shrinkage/myelination and were associated with overexpression of the same transcriptional profile as cortical consolidation. We conclude that normative human brain maturation involves a genetically patterned process of consolidating anatomical network hubs. We argue that developmental variation of this consolidation process may be relevant both to normal cognitive and behavioral changes and the high incidence of schizophrenia during human brain adolescence.

graph theory | partial least squares | myelinogenesis | microarray | magnetization transfer

Adolescence is associated with major behavioral, social, and sexual changes as well as increased risk for many psychiatric disorders (1). However, human brain maturation during adolescence is not yet so well understood. Historically, pioneering studies used histological techniques to show that distinct areas of cortex were differentially myelinated in postmortem examination of perinatal tissue, suggesting "myelinogenesis" as an important process in human brain development (2, 3). MRI can measure human brain development more comprehensively and over a wider age range than is possible for postmortem anatomists. The thickness of human cortex can be reliably and replicably measured by MRI (4), and longitudinal studies have shown that cortical thickness (CT; millimeters) monotonically shrinks over the course of postnatal development, with variable shrinkage rates estimated for different age ranges (5–11; review in ref. 12). CT typically shrinks from about 3.5 mm at age 13 y old (9) to about 2.2 mm at age 75 y old (10, 11). Rates of cortical shrinkage are faster during adolescence (approximately −0.05 mm/y) than in later adulthood or earlier childhood (9).

What does this MRI phenomenon of cortical shrinkage represent at a cellular level? There are broadly two tenable models: pruning and myelination. Basic physical principles of MRI predict

that shorter longitudinal (T1) relaxation times reflect either a reduction in the fraction of "watery" cytoplasmic material, like cell bodies, synapses, or extracellular fluid, or an increase in the fraction of "fatty" myelinated material, like axons. Pruning models propose that cortical shrinkage in adolescence represents loss or remodeling of synapses, dendrites, or cell bodies (13). Myelination models propose that the cortex appears to shrink because of an increasing proportion of myelinated axons, without necessarily implying any loss or change of neuronal material (5).

In the macaque monkey, although the main phase of synaptic pruning and neuronal loss occurs earlier in development (14, 15), there is evidence for further synaptic remodeling during adolescence (16, 17). In rodents, there is histological evidence for increasing intracortical myelination during adolescence, especially at the deeper cytoarchitectonic layers of cortex (V and VI) (18, 19). At a cellular

Significance

Adolescence is a period of human brain growth and high incidence of mental health disorders. Here, we show consistently in two MRI cohorts that human brain changes in adolescence were concentrated on the more densely connected hubs of the connectome (i.e., association cortical regions that mediated efficient connectivity throughout the human brain structural network). Hubs were less myelinated at 14 y but had faster rates of myelination and cortical shrinkage in the 14- to 24-y period. This topologically focused process of cortical consolidation was associated with expression of genes enriched for normal synaptic and myelin-related processes and risk of schizophrenia. Consolidation of anatomical network hubs could be important for normal and clinically disordered adolescent brain development.

NEUROSCIENCE

Fig. 1. Cortical thickness (CT) and magnetization transfer (MT) maps. At 14 y old, primary somatosensory and visual cortices had (*A*) thinner cortex and (*C*) greater MT than association cortical areas. (*F*) Baseline CT (millimeters) and MT (PU) were negatively correlated, confirming that thinner cortex was more myelinated at 14 y old. Globally, over all 308 regions, (*B*) CT decreased linearly with increasing age in the range 14–24 y old, although (*E*) there were regional differences in the rate of cortical shrinkage (ΔCT), with significantly nonzero rates of shrinkage (permutation test; FDR = 0.05) located mainly in the association cortex. (*D*) Globally, MT increased linearly with increasing age in the range 14–24 y old, although (*G*) there were regional differences in the rate of cortical myelination (ΔMT), with significantly nonzero rates of myelination (permutation test; FDR = 0.05) located mainly in the association cortex. (*H*) Rates of change in thickness and MT were negatively correlated, confirming that more rapidly shrinking areas of cortex had faster rates of myelination.

level, this signal likely reflects a developmentally late myelination of efferent axonal segments immediately distal to the axonal hillock of pyramidal cells (20). MRI sequences have been recently developed for myelin mapping in humans (21). These techniques include methods based on magnetization transfer (MT), which have been validated as an MRI marker of myelination by postmortem imaging and histological studies of multiple sclerosis, a demyelinating disorder (22) (details are in *Methods*). It has been shown that primary sensory and motor areas of cortex are more heavily myelinated than association cortical areas, that most cortical areas show progressive increases in myelination over the course of normative development into middle age, and that myelination is concentrated in deeper layers of cortex (21, 23, 24). Association cortical areas have been identified among the highly connected "hubs" of structural brain networks (25), suggesting that differential rates of intracortical myelination might be related to differences between regions in their topological roles as part of the connectome. Developmental changes in structural and functional MRI network topology have been reported (review in ref. 26) but not previously related to measures of cortical shrinkage or myelination. Recently, several studies have linked brain regional gene expression to axonal connectivity in the mouse (27, 28) and functional MRI networks in humans (29, 30), but there have been no previous efforts to investigate genetic mechanisms of adolescent myelination of human cortex.

In this context, we aimed to test three hypotheses: (*i*) that adolescent cortical shrinkage was coupled to intracortical myelination, (*ii*) that adolescent cortical shrinkage/myelination (also known as consolidation) was concentrated anatomically on association cortex and topologically on the most strongly connected regions (hubs) of the human brain anatomical network, and (*iii*) that adolescent consolidation of these connectome hubs was associated with a specific gene expression profile, enriched for neuronal and oligodendroglial

function, and enriched for risk of schizophrenia, a neurodevelopmental disorder with its highest incidence in young adults.

We used quantitative multiparameter mapping (MPM) (31) to test these hypotheses on MRI data acquired from a sample of 297 healthy young people sampled from primary healthcare registers, stratified by age, and balanced for sex in the adolescent age range 14–24 y old, with ~60 participants in each of five age-defined strata: 14–15 y old inclusive, 16–17 y old, 18–19 y old, 20–21 y old, and 22–24 y old (*Methods* and *SI Appendix*, Table S1). From the MRI data, we measured CT (millimeters) and MT [percentage units (PU)] at each of 308 cortical regions for all participants. We used linear models to estimate baseline CT and MT at 14 y old and age-related rates of change in the period from 14 to 24 y old (ΔCT and ΔMT) from data on participants of all ages at each regional node. We explored the relationships between these local cortical MRI markers and a few key metrics of complex network topology that have been widely used in prior neuroimaging and other neuroscience studies (review in ref. 32). We focused on the degree and closeness of each node—as measures of nodal "hubness"—and the community structure of the network—defined as a set of sparsely interconnected modules; details of topological connectome analysis are in *Methods* and *SI Appendix*. We investigated the relationships between gene transcriptional profiles and colocalized MRI (CT and MT) and network topological phenotypes by multivariate analysis of MRI data on 297 adolescents and whole-genome gene expression maps of six adult human brains (postmortem) provided by the Allen Institute for Brain Science (AIBS) (33); details are in *Methods* and *SI Appendix*.

For robustness and generalizability, we first analyzed data from a discovery cohort (*n* = 100; balanced for age and sex as per the sample design) and then replicated all of the key findings in a validation cohort (*n* = 197). Nonidentifiable data and all analyses codes are available at the Neuroscience in Psychiatry Network Cortical Myelination Figshare Repository (details are in *SI Appendix*).

Results

CT and Shrinkage. CT at 14 y of age ranged between 1.93 and 3.8 mm across different cortical areas. Baseline CT was thinnest in primary somatosensory and visual cortices (Fig. 1*A*) (34). In the adolescent period from 14 to 24 y old, there was evidence of significant cortical shrinkage ($r^2 = 0.10$; $P = 0.006$; estimated global rate of shrinkage; $\Delta CT = -0.011$ mm/y) (Fig. 1*B*). Although 289 of 308 nodes exhibited cortical shrinkage ($\Delta CT < 0$), only 79 nodes showed shrinkage that was statistically significant at $P < 0.05$ after false discovery rate (FDR) correction for multiple comparisons (Fig. 1*C*). The regions with the greatest rates of shrinkage were located in association cortex.

Intracortical MT and Myelination. By combining data from neighboring voxels in each regional node, we could estimate regional MT for each depth at submillimeter resolution (4), corresponding approximately to different layers of cortex (Fig. 2*A*). MT was estimated at 10 fractional depths of the cortical ribbon from the pial surface (0% depth) to the gray/white matter (GM/WM) boundary (100% depth) and two infracortical locations 0.4 and 0.8 mm below the GM/WM boundary. At each cortical depth, we estimated baseline MT (at age 14 y old) and adolescent change in MT (over the age range of 14–24 y old). In all regions, as expected, baseline MT increased monotonically as a function of increasing depth from the pial surface, reflecting greater density of myelinated fibers in deeper cortical layers (Fig. 2*B* and Movie S1). However, there was marked regional variability (Fig. 1*C*): areas of primary sensory cortex had greater MT at age 14 y old than association cortical areas.

The rate of adolescent change in MT, ΔMT, was greatest when measured at 70% of the depth of cortex (Fig. 2*D* and Movie S2) [i.e., ~1.9 mm below the pial surface and ~0.8 mm above the boundary with white matter; across all cortical regions: $r^2 = 0.17$; $P < 0.001$; $\Delta MT = 4.98 \times 10^{-3}$ y^{-1} (Fig. 1*D*)]. Seventy percent cortical depth corresponds approximately to the level of lamina V

Whitaker et al.
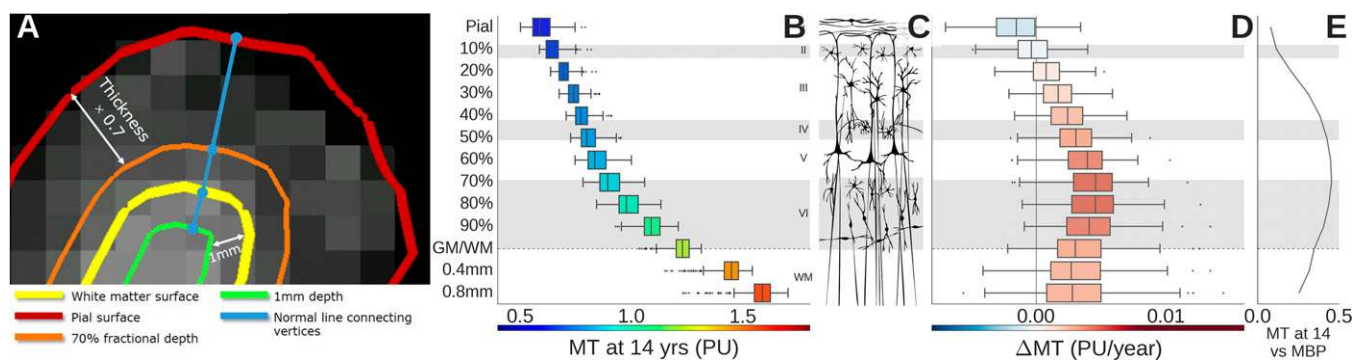
Fig. 2. Magnetization transfer (MT) mapping of intracortical myelination. (*A*) The schematic highlights estimation of MT on a contour (orange line) located at 70% of the cortical depth from the pial surface and another contour (green line) located 1 mm below the boundary between gray matter and white matter (yellow line). (*C*) These distances and others can be located approximately in the context of cytoarchitectonic lamina of human neocortex. (*B*) Baseline MT increases monotonically with distance from the pial surface, but (*D*) the age-related increase in MT (ΔMT) was greatest at 70% cortical depth. (*E*) The correlation between baseline MT and *MBP* gene expression was also strongest at 70% cortical depth. Boxes represent the medians and interquartile ranges over all 308 regions at each depth.

and VI, comprising the internal layer of pyramidal or projection neurons (Fig. 2*C*). There was marked regional variability in the rates of myelination: regions with the greatest rates of myelination were located in association cortices (Fig. 1*G*).

In light of these complementary anatomical and developmental profiles of CT and MT, it is not surprising that there was a strong negative correlation between baseline CT and MT ($r^2 = 0.43$; $P < 0.001$; $\beta = -0.120$ PU/mm) (Fig. 1*F*) and a strong negative correlation between rates of cortical shrinkage and intracortical myelination ($r^2 = 0.22$; $P < 0.001$; $\beta = -0.126$ PU/mm) (Fig. 1*H*). Adolescent cortical shrinkage was significantly but not entirely mediated by age-dependent changes in MT (*SI Appendix*, Fig. S1*E*), indicating that myelination is necessary but not sufficient to account for cortical shrinkage.

Internal Replication. All of the results reported so far were based on analysis of the discovery cohort ($n = 100$; 20 in each of five age bins; 50 females), and all were closely replicated in the validation cohort ($n = 197$; ~40 in each of five age bins; 98 females) (*SI Appendix*, Figs. S1 and S2). Because the validation cohort had twice as many participants, it conferred greater statistical power to test hypotheses. We henceforth focus on the most precise estimates of CT and MT (at 70% cortical depth) estimated from the total sample ($n = 297$; 60 per age bin; 30 females), although all additional analyses were also reproduced separately for the discovery and validation cohorts (*SI Appendix*, Figs. S3 and S4).

Genomic Patterning of Adolescent Cortical Consolidation. To elucidate the molecular mechanisms of local change in CT and MT, we explored the association between these MRI markers and regional gene expression profiles from human adult brain microarray datasets provided by the AIBS (33). For example, baseline MT was correlated with regional expression of the gene for myelin basic protein (*MBP*) across cortex (Fig. 2*E*), confirming that the MT signal is indicative of myelin content (22). The association was strongest at 70% cortical depth ($r^2 = 0.21$; $P < 0.001$; $\beta = 0.0723$) (*SI Appendix*, Fig. S3*A*).

To explore analogous associations between all four cortical MRI metrics and all 20,737 genes measured in the AIBS microarrays, at each of 308 regions, we used the multivariate, dimension-reducing technique of partial least squares (PLS) (35). This analysis defined a few PLS components, which were the linear combinations of the weighted gene expression scores (predictor variables) that were most strongly correlated with one or more of the MRI markers (response variables; CT at 14 y, MT at 14 y, ΔCT, and ΔMT).

The top two PLS components explained 28% of the variance in the MRI response variables (permutation test; $P < 0.001$). The first partial least squares component (PLS1) (Fig. 3*A*) represented a significant association between a rostrocaudally patterned gene expression profile and baseline measures of CT and MT at 14 y old (Fig. 3 *B* and *C* and *SI Appendix*, Fig. S5). The second independent partial least squares component (PLS2) (Fig. 3*D*) represented a significant association between a dorsoventrally patterned gene expression profile and measures of adolescent cortical shrinkage and myelination (Fig. 3 *E* and *F*). Dataset S1 has a full list of significantly over- or underexpressed genes represented by the first two PLS components.

Focusing on the gene expression profile defined by PLS2, because it was specifically associated with adolescent cortical shrinkage and intracortical myelination, we found that this transcriptional signature was significantly enriched in genes relating to synaptic transmission ($P < 0.001$), regulation of glutamatergic signaling ($P < 0.001$), and potassium ion channels ($P < 0.001$) (36) (*SI Appendix*, Fig. S3*G*). We also found that the transcriptional profile associated with association cortical consolidation was significantly enriched for an oligodendroglial gene set ($P < 0.001$) (37) (*SI Appendix*, Fig. S3*F*) as well as a set of genes robustly associated with risk for schizophrenia, a neurodevelopmental disorder ($P < 0.001$) (38) (*SI Appendix*, Fig. S3*G*).

Adolescent Cortical Consolidation and the Connectome. We used the measurements of CT on the total sample to estimate the mean structural covariance matrix, representing the pairwise correlation of CT between each possible pair of 308 regions. This matrix was thresholded to construct a binary graph or structural covariance network that had a complex topology, consistent with many prior reports of human anatomical connectomes (*SI Appendix*, Fig. S6) (39).

Globally, the network was small world with hubs (indicated by a fat-tailed degree distribution), a modular community structure, and a rich club or core of densely interconnected high-degree nodes or hubs, which were located primarily in frontal and parietal association cortices (Fig. 4*A* and *SI Appendix*, Fig. S6). At a nodal level of analysis, high-degree hub nodes also had high closeness centrality, indicating short path length of connections to other nodes in the network (Fig. 4*B*), as well as long physical distance of connections. Cortical shrinkage was faster for topologically central hubs with long-distance connections (Fig. 4*C*) (degree: $r^2 = 0.14$; $P < 0.001$; $\beta = -1.48 \times 10^{-3}$ mm^{-1}; closeness: $r^2 = 0.18$; $P < 0.001$; $\beta = -4.91$ mm^{-1}; distance: $r^2 = 0.09$; $P < 0.001$; $\beta = -0.81 \times 10^{-3}$). Intracortical myelination rates were also faster for long-distance hubs (Fig. 4*D*) (degree: $r^2 = 0.07$; $P < 0.001$; $\beta = 3.81 \times 10^3$ PU^{-1}; closeness: $r^2 = 0.13$; $P < 0.001$; $\beta = 14.8$ PU^{-1}; distance: $r^2 = 0.21$; $P < 0.001$; $\beta = 4.42 \times 10^3$ mm/PU).

We found that degree, closeness, and connection distance were also positively correlated with the pattern of gene expression associated with adolescent change in cortical structure (PLS2; degree: $r^2 = 0.21$; $P < 0.001$; $\beta = 178$; closeness: $r^2 = 0.26$; $P < 0.001$; $\beta = 572 \times 10^{-3}$; distance: $r^2 = 0.15$; $P < 0.001$; $\beta = 100$ mm) (Fig. 4*E*). In
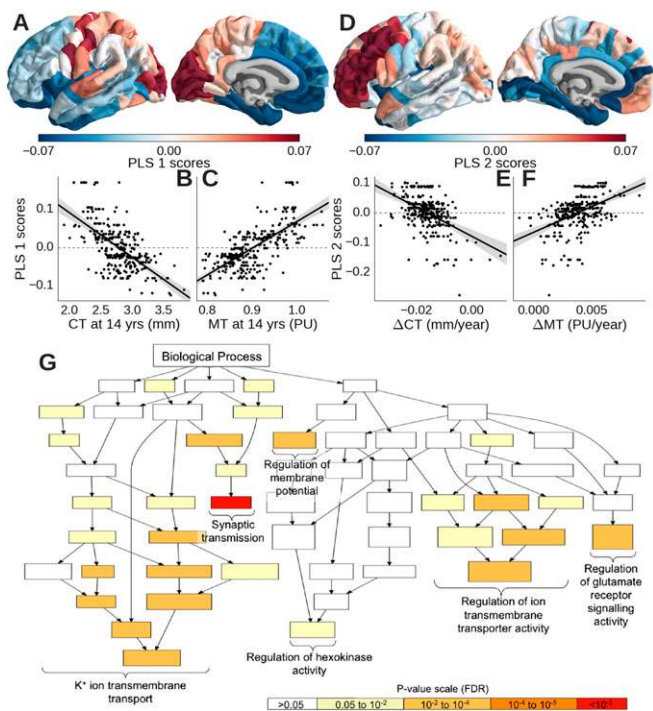
Fig. 3. Distinct gene expression profiles were specifically associated with CT and MT at 14 y old or adolescent processes of cortical consolidation. PLS1 identified a profile of genes that were (*A*) overexpressed in occipital and somatosensory cortices, (*B*) negatively correlated with baseline CT, and (*C*) positively correlated with baseline MT. PLS2 identified a profile of genes that were (*D*) overexpressed in prefrontal cortex, (*E*) negatively correlated with adolescent cortical shrinkage (ΔCT), and (*F*) positively correlated with adolescent intracortical myelination (ΔMT). (*G*) PLS2 was enriched for genes functionally related to synaptic transmission, glutamatergic signaling, and potassium ion channels (color-coded by *P* value for significant enrichment) in the gene ontology of biological processes.

changes in MT, corresponding approximately to the boundary between layers V (internal pyramid) and VI, further suggests that adolescent intracortical myelination may be concentrated on the proximal segments of efferent projections from pyramidal neurons (20).

Although adolescent intracortical myelination was greatest in areas that showed fastest rates of cortical shrinkage, it did not entirely explain age-related changes in CT. Likewise, although the gene expression profile associated with adolescent change was enriched for genes related to oligodendroglial function, it was also significantly enriched for neuronal genes, especially those implicated in remodeling of synapses or transport of glutamate-containing vesicles. Thus, it seems plausible that genetically programmed processes of synaptic remodeling act together with locally coupled processes of intracortical myelination to consolidate synaptic and axonal connectivity of association cortical areas in adolescence. The set of gene transcription markers most strongly associated with this late maturational process (44) was enriched for genes known to confer risk for schizophrenia (38), generating the hypothesis that deviation from the normative developmental trajectory of cortical hub consolidation could be an intermediate phenotype underlying the high incidence of the clinical phenotype of schizophrenia in young people.

However, we note some important caveats that mandate additional critical testing of these results and their hypothetical implications. First, the gene expression profiles used in this analysis were measured in six postmortem adult brains (mean age = 43 y old). Brain regional gene expression is known to change somewhat over the two decades approximately intervening between the oldest subject in the MRI dataset and the average age of the subjects in the genomic dataset (45). Any such age-related changes in gene expression will have confounded our analysis of the association between imaging and genomic variables. We might expect this age disparity to reduce the statistical power to detect true MRI/mRNA associations rather than inflate the probability of false positive associations. Nonetheless, the genomic analysis of developmental MRI phenotypes would certainly be stronger in the future if it was informed by age-matched

contrast, these metrics were not so strongly correlated with the pattern of gene expression associated with cortical structure at 14 y old (PLS1; degree: $r^2 < 0.01$; $P = 0.904$; $\beta = -2.36$; closeness: $r^2 < 0.01$; $P = 0.892$; $\beta = 9.39 \times 10^{-3}$; distance: $r^2 = 0.02$; $P = 0.02$; $\beta = -35.2$ mm).
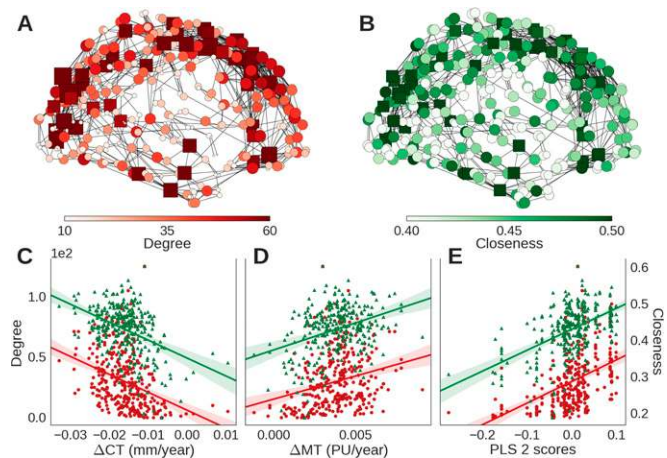
Discussion

We have shown that adolescent cortical shrinkage is related to changes in intracortical MT in humans. This observation supports myelination models of shrinkage and, more generally, confirms association cortical myelinogenesis as a key neurodevelopmental process in adolescence. Our baseline MT-based myelination maps (Figs. 1 and 2) show a high degree of correspondence with previous myelin maps based on alternative MRI parameters (23, 24, 40–42). Across modalities, the highest levels of myelin are located in areas of primary isocortex comprising many large pyramidal cells, which are the principal targets and sources of axonal projections (43). However, arguably, the strongest evidence that MT is representative of myelin content in these data is that MT was highly correlated with regional expression of the gene for *MBP* and that the set of genes most strongly correlated with adolescent change in MT was significantly enriched for oligodendroglia-related genes.

We interpret our findings as indicating that adolescent cortical myelination was greatest in association areas, which were least myelinated at age 14 y old. It is plausible, although not directly shown by these data, that specialized motor and sensory cortices may show faster rates of intracortical MT change compared with association cortex at earlier stages of development. This prediction would be compatible with the idea, dating back to Flechsig (2), that association cortical areas are the focus of a relatively late wave of myelinogenesis. The intracortical location of strongest maturational

Fig. 4. Hubs of the connectome were located in regions with faster rates of cortical consolidation and associated with the same gene expression profile as consolidation. The structural covariance network comprised hubs with (*A*) high degree centrality and (*B*) high closeness centrality that were concentrated anatomically in association cortical areas; in both *A* and *B*, nodes are colored and sized by the corresponding centrality metric, and square nodes represent members of the rich club. Both degree (red) and closeness centrality (green) were (*C*) negatively correlated with cortical shrinkage (ΔCT) and (*D*) positively correlated with adolescent increase in myelination (ΔMT). (*E*) The gene expression profile associated with adolescent cortical consolidation (PLS2 from Fig. 3) was also significantly associated with degree and closeness centrality.

regional gene expression profiles (such data are not currently available). Second, the MRI changes that we have interpreted developmentally are estimated from cross-sectional data. A longitudinal design incorporating multiple repeated MRI scans over time would provide a more secure basis for estimation of age-related changes attributable to the developmental maturation of individual brains. Third, we have not presented any evidence that people at risk for schizophrenia do, indeed, show abnormal cortical hub consolidation, although we note that there is prior evidence for abnormal CT, MT, and cortical shrinkage in patients with schizophrenia (46, 47). Future longitudinal studies of network development (and ideally, also gene expression) in young people genetically or environmentally at risk for schizophrenia will be required to test the pathogenic role of hub consolidation more definitively.

It is well known that brain networks generally have complex topological properties, including hubs, modules, and rich clubs (39, 48). We replicated these findings by graph theoretical analysis of structural covariance networks (derived from the CT measurements), showing that topologically central nodes had higher rates of adolescent shrinkage and myelination and higher levels of gene expression associated with cortical consolidation. In a sense, this result is not surprising given our earlier data showing that the coupled changes in CT and MT were greatest in association cortex and prior studies showing that network hubs of the structural brain connectome are disproportionately located in association cortex (39). It suggests that adolescent cortical consolidation is topologically targeted to optimize the performance of network hubs. For example, synaptic remodeling and intracortical myelination of cortical hubs might be expected to minimize the conduction time for axonal propagation of electrical signals or enhance the synchronization of oscillations across anatomically distributed cortical areas (49). These physiological implications of connectome hub consolidation would hypothetically favor more integrative functional network topology and dynamics, which are known to be important for later-maturing, "higher-order" cognitive functions (50).

We predict that age-related cortical consolidation of human cortical network hubs will prove to be relevant to the normal acquisition of cognitive and behavioral skills during the adolescent transition from childhood to adulthood and may also prove to be implicated in the clinical emergence of neurodevelopmental and psychiatric disorders, such as schizophrenia, in young people (1, 3).

Methods

Design. In total, 2135 healthy young people in the age range 14–24 y old were recruited from schools, colleges, National Health Service (NHS) primary care services, and via direct advertisement in north London and Cambridgeshire. To populate the (secondary) MRI cohort, 300 participants were subsampled from the primary cohort (conserving sex and ethnicity balance), with $n = 60$ in each of five age strata. Additional detail and exclusion criteria are in *SI Appendix*. Participants provided informed written consent for each aspect of the study, and parental consent was obtained for those aged 14–15 y old. The study was ethically approved by the National Research Ethics Service and conducted in accordance with NHS research governance standards.

MRI Data Acquisition. All scans were acquired using the MPM sequence (31) implemented on three identical 3T whole-body MRI systems (Magnetom TIM Trio; VB17 software version; Siemens Healthcare): two located in Cambridge and one located in London. Between-site reliability and tolerability of all MRI procedures were satisfactorily assessed by a pilot study of five healthy volunteers each scanned for ~25 min at each site (31). The between-site bias was less than 3% and the between-site coefficient of variation was less than 8% for both longitudinal relaxation rate (R1) and MT parameters (31). R1 and MT were quantified in Matlab (The MathWorks, Inc.) using SPM8 (www.fil.ion.ucl.ac.uk/spm) and custom tools; details are in *SI Appendix*.

Estimation of Regional CT and MT. The cortical surface for each participant was reconstructed from the R1 image by the following steps: skull stripping (51), segmentation of cortical gray and white matter (52), separation of the two hemispheres and subcortical structures (52–54), and finally, construction of a smooth representation of the gray/white interface and the pial surface (52). We used FreeSurfer v5.3.0 software to implement these processes

(surfer.nmr.mgh.harvard.edu). After quality control, three participants had to be excluded from the analyses because of movement artifacts, which prevented accurate surface reconstructions. We used a backtracking algorithm (55) to parcellate 66 regions defined by sulcogyral criteria in the Desikan–Killiany atlas (56) into 308 contiguous parcels of approximately equal area (500 mm²) across both hemispheres in standard space (*SI Appendix*, Fig. S2A). This parcellation template was then transformed to the native space of each participant's image to minimize geometric deformation of the MRI data and prevent age-related bias (57) before estimation of CT of each region. To localize cortical myelination at a spatial resolution corresponding approximately to the scale of six lamina of neocortex, at each regional node, we estimated MT at each of 11 equidistant points on the normal line from the GM/WM boundary (fractional cortical depth = 100%) to the pial surface (0%). By measuring MT at depths defined in proportion to CT, we aimed to adjust the measurements for variation in absolute CT between different regions and as a function of age. We additionally estimated MT at two locations, consistently defined as 0.4 and 0.8 mm below the GM/WM boundary, to sample the dense myelination of central white matter as a point of comparison for intracortical MT (details are in Fig. 2 and *SI Appendix*).

Gene Expression Dataset. Microarray data for five male and one female donors with a mean age of 42.5 y old were available from the AIBS (33) (human.brain-map.org). We matched the centroids of the regions of the MRI parcellation to the closest regional gene expression profile. Microarray data were averaged across all samples from all donors in the matching anatomical region across both hemispheres. The data were also averaged across probes corresponding to the same gene, excluding probes that were not matched to gene symbols in the AIBS data. Two MRI regions were excluded, because both the mean and the range of gene expression values in these regions were outliers compared with the other cortical regions of interest. The final output was a matrix of Z-scored expression values for each of 20,737 genes estimated in 306 MRI regions (details are in *SI Appendix*). Gene expression data for individual genes, such as *MBP*, were obtained from the appropriate row of this matrix. Similarly, gene expression values for larger gene sets of interest were extracted from the whole-genome data. These hypothetically motivated gene sets included 94 genes that were identified as oligodendrocyte-specific by Cahoy et al. (37) and 349 protein-coding genes recently identified as schizophrenia risk genes (38), of which 312 were successfully matched to genes in the AIBS dataset.

Structural Covariance and Network Analyses. The structural covariance matrix comprised the pairwise correlations of CT for all possible pairs of regions in the parcellation template. Binary graphs were constructed to be node-connected, with a connection density of 10% (39). From this graphical model of the connectome, we estimated two measures of topological centrality at each node: degree and closeness. These metrics are representative of the more general concept of nodal centrality, and they are strongly correlated. We also estimated the connection distance as the mean of the Euclidean distance of all of the nonzero edges at each node. On average over all nodes, we estimated clustering and global efficiency and combined these measures of network segregation and integration, respectively, to estimate the small worldness of the global network (58). The community structure of the graph was "nearly decomposed" by maximization of modularity (59) into a set of sparsely interconnected modules or subgraphs. The core/periphery structure of the graph was defined as a small rich club or core of highly interconnected hubs embedded in a larger set of more peripheral nodes. Details are in *SI Appendix*.

Statistical Analyses. At each regional node, we fitted a simple linear regression model across all participants to estimate the gradient (ΔCT and ΔMT) and intercept or baseline (CT and MT) for each MRI measurement. For MT, the same model was fitted separately at each depth level between the pial surface and 0.8 mm below the GM/WM boundary. The null hypothesis of zero age-related change in ΔCT or ΔMT was tested globally on average over all regions and at each region individually, controlling the FDR at 5% to correct for multiple comparisons entailed by regional analysis. PLS regression on the gene expression matrix was used to identify the linear combinations of genes that best predicted the response variables (CT, MT, ΔCT, and ΔMT). The statistical significance of the goodness of fit of the first two PLS components was tested with two-tailed $\alpha = 0.05$ by 1,000 permutations of the response variables. The error in estimation of the weight of each gene on each PLS component was assessed by bootstrapping, and the ratio of the weight of each gene to its bootstrap SE was used to rank the genes according to their contribution to each PLS component. We used gene ontology enrichment analysis tools to identify and summarize annotations corresponding to biological processes that were significantly overrepresented (FDR = 5%) (details are in *SI Appendix*). We

predicted hypothetically that the transcriptional profile strongly associated with adolescent cortical consolidation (PLS2) should be enriched for genes associated with oligodendroglia (37) or risk for schizophrenia (38). We tested for significant enrichment by a permutation test of the normalized bootstrap weight of each gene in PLS1 and PLS2 summed over all genes in the set.

1. Paus T, Keshavan M, Giedd JN (2008) Why do many psychiatric disorders emerge during adolescence? *Nat Rev Neurosci* 9(12):947–957.
2. Flechsig P (1901) Developmental (myelogenetic) localisation of the cerebral cortex in the human subject. *Lancet* 158(4077):1027–1030.
3. Miller DJ, et al. (2012) Prolonged myelination in human neocortical evolution. *Proc Natl Acad Sci USA* 109(41):16480–16485.
4. Rosas HD, et al. (2002) Regional and progressive thinning of the cortical ribbon in Huntington's disease. *Neurology* 58(5):695–701.
5. Sowell ER, et al. (2004) Longitudinal mapping of cortical thickness and brain growth in normal children. *J Neurosci* 24(38):8223–8231.
6. Gogtay N, et al. (2004) Dynamic mapping of human cortical development during childhood through early adulthood. *Proc Natl Acad Sci USA* 101(21):8174–8179.
7. Raznahan A, et al. (2011) How does your cortex grow? *J Neurosci* 31(19):7174–7177.
8. Wierenga LM, Langen M, Oranje B, Durston S (2014) Unique developmental trajectories of cortical thickness and surface area. *Neuroimage* 87:120–126.
9. Zhou D, Lebel C, Treit S, Evans A, Beaulieu C (2015) Accelerated longitudinal cortical thinning in adolescence. *Neuroimage* 104:138–145.
10. Salat DH, et al. (2004) Thinning of the cerebral cortex in aging. *Cereb Cortex* 14(7):721–730.
11. Storsve AB, et al. (2014) Differential longitudinal changes in cortical thickness, surface area and volume across the adult life span: Regions of accelerating and decelerating change. *J Neurosci* 34(25):8488–8498.
12. Khundrakpam BS, Lewis JD, Zhao L, Chouinard-Decorte F, Evans AC (2016) Brain connectivity in normally developing children and adolescents. *Neuroimage* 134:192–203.
13. Huttenlocher PR, Dabholkar AS (1997) Regional differences in synaptogenesis in human cerebral cortex. *J Comp Neurol* 387(2):167–178.
14. Bourgeois JP, Goldman-Rakic PS, Rakic P (1994) Synaptogenesis in the prefrontal cortex of rhesus monkeys. *Cereb Cortex* 4(1):78–96.
15. Finlay BL, Slattery M (1983) Local differences in the amount of early cell death in neocortex predict adult local specializations. *Science* 219(4590):1349–1351.
16. Rakic P, Bourgeois JP, Eckenhoff MF, Zecevic N, Goldman-Rakic PS (1986) Concurrent overproduction of synapses in diverse regions of the primate cerebral cortex. *Science* 232(4747):232–235.
17. Bourgeois JP, Rakic P (1993) Changes of synaptic density in the primary visual cortex of the macaque monkey from fetal to adult stage. *J Neurosci* 13(7):2801–2820.
18. Mengler L, et al. (2014) Brain maturation of the adolescent rat cortex and striatum: Changes in volume and myelination. *Neuroimage* 84:35–44.
19. Hammelrath L, et al. (2016) Morphological maturation of the mouse brain: An in vivo MRI and histology investigation. *Neuroimage* 125:144–152.
20. Tomassy GS, et al. (2014) Distinct profiles of myelin distribution along single axons of pyramidal neurons in the neocortex. *Science* 344(6181):319–324.
21. Glasser MF, Goyal MS, Preuss TM, Raichle ME, Van Essen DC (2014) Trends and properties of human cerebral cortex: Correlations with cortical myelin content. *Neuroimage* 93(Pt 2):165–175.
22. Schmierer K, et al. (2007) Quantitative magnetization transfer imaging in postmortem multiple sclerosis brain. *J Magn Reson Imaging* 26(1):41–51.
23. Grydeland H, Walhovd KB, Tamnes CK, Westlye LT, Fjell AM (2013) Intracortical myelin links with performance variability across the human lifespan: Results from T1- and T2-weighted MRI myelin mapping and diffusion tensor imaging. *J Neurosci* 33(47):18618–18630.
24. Shafee R, Buckner RL, Fischl B (2015) Gray matter myelination of 1555 human brains using partial volume corrected MRI images. *Neuroimage* 105:473–485.
25. Sporns O, Honey CJ, Kötter R (2007) Identification and classification of hubs in brain networks. *PLoS One* 2(10):e1049.
26. Vértes PE, Bullmore ET (2015) Annual research review: Growth connectomics—the organization and reorganization of brain networks during normal and abnormal development. *J Child Psychol Psychiatry* 56(3):299–320.
27. Rubinov M, Ypma RJF, Watson C, Bullmore ET (2015) Wiring cost and topological participation of the mouse brain connectome. *Proc Natl Acad Sci USA* 112(32):10032–10037.
28. Fulcher BD, Fornito A (2016) A transcriptional signature of hub connectivity in the mouse connectome. *Proc Natl Acad Sci USA* 113(5):1435–1440.
29. Richiardi J, et al.; IMAGEN consortium (2015) Correlated gene expression supports synchronous activity in brain networks. *Science* 348(6240):1241–1244.
30. Vértes PE, et al. (2016) Gene transcription profiles associated with inter-modular hubs and connection distance in human fMRI networks. *Philos Trans R Soc Lond B Biol Sci*, in press.
31. Weiskopf N, et al. (2013) Quantitative multi-parameter mapping of R1, PD(*), MT, and R2(*) at 3T: A multi-center validation. *Front Neurosci* 7:95.
32. Fornito A, Zalesky A, Bullmore ET (2016) *Fundamentals of Brain Network Analysis* (Academic, San Diego).
33. Hawrylycz MJ, et al. (2012) An anatomically comprehensive atlas of the adult human brain transcriptome. *Nature* 489(7416):391–399.
34. Wagstyl K, Ronan L, Goodyer IM, Fletcher PC (2015) Cortical thickness gradients in structural hierarchies. *Neuroimage* 111:241–250.
35. Abdi H (2010) Partial least squares regression and projection on latent structure regression (PLS Regression). *Wiley Interdiscip Rev Comput Stat* 2(1):97–106.
36. Eden E, Navon R, Steinfeld I, Lipson D, Yakhini Z (2009) GOrilla: A tool for discovery and visualization of enriched GO terms in ranked gene lists. *BMC Bioinformatics* 10(1):48.
37. Cahoy JD, et al. (2008) A transcriptome database for astrocytes, neurons, and oligodendrocytes: A new resource for understanding brain development and function. *J Neurosci* 28(1):264–278.
38. Ripke S, et al.; Schizophrenia Working Group of the Psychiatric Genomics Consortium (2014) Biological insights from 108 schizophrenia-associated genetic loci. *Nature* 511(7510):421–427.
39. Alexander-Bloch A, Giedd JN, Bullmore E (2013) Imaging structural co-variance between human brain regions. *Nat Rev Neurosci* 14(5):322–336.
40. Glasser MF, Van Essen DC (2011) Mapping human cortical areas in vivo based on myelin content as revealed by T1- and T2-weighted MRI. *J Neurosci* 31(32):11597–11616.
41. Eickhoff S, et al. (2005) High-resolution MRI reflects myeloarchitecture and cytoarchitecture of human cerebral cortex. *Hum Brain Mapp* 24(3):206–215.
42. Lutti A, Dick F, Sereno MI, Weiskopf N (2014) Using high-resolution quantitative mapping of R1 as an index of cortical myelination. *Neuroimage* 93(Pt 2):176–188.
43. Helbling S, et al. (2015) Structure predicts function: Combining non-invasive electrophysiology with in-vivo histology. *Neuroimage* 108:377–385.
44. Fjell AM, et al. (2015) Development and aging of cortical thickness correspond to genetic organization patterns. *Proc Natl Acad Sci USA* 112(50):15462–15467.
45. Kang HJ, et al. (2011) Spatio-temporal transcriptome of the human brain. *Nature* 478(7370):483–489.
46. Alexander-Bloch AF, et al. (2014) Abnormal cortical growth in schizophrenia targets normative modules of synchronized development. *Biol Psychiatry* 76(6):438–446.
47. Foong J, et al. (2001) Neuropathological abnormalities in schizophrenia: Evidence from magnetization transfer imaging. *Brain* 124(Pt 5):882–892.
48. Bullmore E, Sporns O (2009) Complex brain networks: Graph theoretical analysis of structural and functional systems. *Nat Rev Neurosci* 10(3):186–198.
49. Salami M, Itami C, Tsumoto T, Kimura F (2003) Change of conduction velocity by regional myelination yields constant latency irrespective of distance between thalamus and cortex. *Proc Natl Acad Sci USA* 100(10):6174–6179.
50. Zatorre RJ, Fields RD, Johansen-Berg H (2012) Plasticity in gray and white: Neuroimaging changes in brain structure during learning. *Nat Neurosci* 15(4):528–536.
51. Ségonne F, et al. (2004) A hybrid approach to the skull stripping problem in MRI. *Neuroimage* 22(3):1060–1075.
52. Dale AM, Fischl B, Sereno MI (1999) Cortical surface-based analysis. I. Segmentation and surface reconstruction. *Neuroimage* 9(2):179–194.
53. Fischl B, et al. (2002) Whole brain segmentation: Automated labeling of neuroanatomical structures in the human brain. *Neuron* 33(3):341–355.
54. Fischl B, et al. (2004) Sequence-independent segmentation of magnetic resonance images. *Neuroimage* 23(Suppl 1):S69–S84.
55. Romero-Garcia R, Atienza M, Clemmensen LH, Cantero JL (2012) Effects of network resolution on topological properties of human neocortex. *Neuroimage* 59(4):3522–3532.
56. Desikan RS, et al. (2006) An automated labeling system for subdividing the human cerebral cortex on MRI scans into gyral based regions of interest. *Neuroimage* 31(3):968–980.
57. Ghosh SS, et al. (2010) Evaluating the validity of volume-based and surface-based brain image registration for developmental cognitive neuroscience studies in children 4 to 11 years of age. *Neuroimage* 53(1):85–93.
58. Latora V, Marchiori M (2001) Efficient behavior of small-world networks. *Phys Rev Lett* 87(19):198701.
59. Blondel VD, Guillaume J-L, Lambiotte R, Lefebvre E (2008) Fast unfolding of communities in large networks. *J Stat Mech Theory Exp* 2008(10):P10008 (abstr).

Whitaker et al.